

**NITROGEN DOPED CARBON CATALYST FOR THE OXYGEN
REDUCTION REACTION TO BE USED FOR METHANE PARTIAL
OXIDATION**

by

Andrew K. Craft

A thesis submitted to the Faculty of the University of Delaware in partial fulfillment of the requirements for the degree of Master of Chemical Engineering

Summer 2017

© 2017 Andrew K. Craft
All Rights Reserved

**NITROGEN DOPED CARBON CATALYST FOR THE OXYGEN
REDUCTION REACTION TO BE USED FOR METHANE PARTIAL
OXIDATION**

by

Andrew K. Craft

Approved: _____
Feng Jiao, Ph.D
Professor in charge of thesis on behalf of the Advisory Committee

Approved: _____
Eric M. Furst, Ph.D
Chair of the Department of Chemical and Biomolecular Engineering

Approved: _____
Babatunde A. Ogunaike, Ph.D.
Dean of the College of Engineering

Approved: _____
Ann L. Ardis, Ph.D.
Senior Vice Provost for Graduate and Professional Education

ACKNOWLEDGMENTS

First of all, I would like to thank my advisor, Dr. Feng Jiao, for his support and guidance throughout the course of my thesis work. He has given me the opportunity to pursue interesting research directions. His energetic pursuit of scientific exploration and willingness to consider new ideas have truly inspired me.

I would like to thank all the members of the Jiao group for making my time here more interesting by providing stimulating conversations, both scientific and non-scientific, as well as help and guidance throughout the work: Matt Jouny, Wesley Luc, Charles Collins, Emily Jeng, Dr. Jonathon Rosen, and Dr. Qi Lu.

I would also like to thank those from outside the department who have given help and guidance: Gerald Poirier at the Advanced Material Characterization Lab for his help with XRD, CHNS Elementar Cube, and Cary UV Vis and Gene Wildonger from Mechanical Engineering for his help with the design and laser cutting of the micro flow cell.

I would like to thank my incoming classmates for camaraderie and friendship. Without you guys I certainly would not be in the position I am in today. Thank you Pierre Desir for being a friend and invaluable resource. I cannot imagine that I would have been able to accomplish the things that I have without your friendship. I will miss the conversations about NY, beer, and sports while eating *Hot Bagels*.

Thank you to my family, especially my parents. Your pursuit and passion has inspired me since day one, and will continue to do so in the future. My friends and professors from SUNY Buffalo, without you, I wouldn't be in this position.

Lastly, I would like to thank my longtime girlfriend, Kyle, for her love and support, she has always been there for me, pushing me to be the best I can be. You have stuck with me for 6 years, and your dedication and passion to Nursing has inspired me, and will do so in the future.

TABLE OF CONTENTS

LIST OF TABLES	vii
LIST OF FIGURES	viii
ABSTRACT	x

Chapter

1	INTRODUCTION	1
1.1	Methane Activation	1
1.2	Partial Oxidation of Methane	4
1.3	Hydrogen Peroxide	7
2	METHODS	13
2.1	Preparation of KIT-6	13
2.2	Preparation of Nitrogen Doped Carbon Catalyst	13
2.3	Electrochemical Testing	14
2.3.1	Rotating Disk Electrode	14
2.3.2	Koutecky-Levich Plots	15
2.3.3	Electrochemical Surface Area	16
2.3.4	Micro Flow Cell	16
2.3.5	Chronoamperometry Testing	17
2.3.6	Potassium Titanium (IV) Oxalate Concentration Method	18
2.4	Characterization Techniques	19
3	NITROGEN DOPED CARBON CATALYST SYNTHESIS AND CHARACTERIZATION	20
3.1	Nitrogen Doped Carbon	20
3.2	Nanocasting	20
3.3	KIT-6	22
3.3.1	Powder X-Ray Diffraction	22
3.3.2	N ₂ Adsorption	23
3.4	Synthesized NDC Catalyst	24

3.4.1	N ₂ Adsorption	24
3.4.2	SEM Micrographs	25
3.4.3	Elemental Analysis	25
3.4.4	Electrochemical Surface Area / Double Layer Capacitance	25
4	OXYGEN REDUCTION REACTION EXPERIMENTS	28
4.1	Oxygen Reduction Reaction	28
4.2	Rotating Disk Electrode	28
4.2.1	Koutecky-Levich	31
4.2.2	Partial Current Densities.....	33
5	MICRO FLOW CELL.....	36
5.1	Design.....	36
5.2	Initial Testing.....	39
5.3	Revised Testing	40
6	CONCLUSIONS AND RECOMMENDATIONS.....	43
6.1	Conclusions	43
6.1.1	NDC Catalyst.....	43
6.1.2	Oxygen Reduction	44
6.1.3	Micro Flow Cell	45
6.2	Recommendations	45
	REFERENCES.....	47
	Appendix	
	COPYRIGHT PERMISSIONS	53

LIST OF TABLES

Table 4.1: Selectivity of NDC_80 and NDC_100.....	32
--	----

LIST OF FIGURES

Figure 1.1: U.S. Methane Emissions, by source, 2014 ⁸	1
Figure 1.2: World Anthropogenic Methane Emissions ⁹	2
Figure 1.3: Catalytic cycle for the oxidation of Methane using Hydrogen Peroxide ¹⁶	6
Figure 2.1: Micro Flow Cell Reactor	17
Figure 3.1: Nanocasting process	21
Figure 3.2: A) XRD diffractogram of KIT-6_100, B) Literature KIT-6 diffractogram used for comparison. Adapted with permission from Pirez, C.; Caderon, J.-M.; Dacquin, J.-P.; Lee, A. F.; Wilson, K., Tunable KIT-6 mesoporous sulfonic acid catalysts for fatty acid esterification. <i>ACS catalysis</i> 2012 , 2 (8), 1607-1614. Copyright 2012 American Chemical Society ⁵⁴	22
Figure 3.3: N ₂ BJH Desorption pore size distribution of KIT-6.....	23
Figure 3.4: N ₂ BJH Desorption pore size distribution of NDC Catalyst	24
Figure 3.5: (A,B) SEM micrographs of synthesized NDC catalyst	25
Figure 3.6: (A,C,E) CV scans in non-faradaic area of ORR Reaction for NDC_80, NDC_100, and NDC_120, (B,D,F) Linearized plots to determine double layer capacitance	27
Figure 4.1: LSV Scan of NDC_80, NDC_100, and NDC_120	29
Figure 4.2: Koutecky-Levich plots at various potentials for A) NDC_80 and B) NDC_100.....	31
Figure 4.3: Total and partial current density of NDC_80 and NDC_100.....	33
Figure 4.4: Typical plot of current vs potential at varying rotation speeds	35
Figure 5.1: Consutructed flow cell.....	37

Figure 5.2: Oxidized graphite electrode.....	39
Figure 5.3: Chronoamperometry testing at 0.12 V RHE	39
Figure 5.4: Concentration and Efficiency using Ir on Ti Mesh as the anode	40
Figure 5.5: Revised flow cell schematic	41
Figure 5.6: Concentration and efficiency using Ir sprayed on membrane as the anode	42

ABSTRACT

Methane (CH_4) is a plentiful, naturally occurring hydrocarbon, and the main constituent of natural gas. Due to its abundance, it has been well studied as both a feedstock for chemical production and as a fuel. Recently, methane has become of interest due to its release into the atmosphere as a result of human activities. Rather than capture and use methane, companies opt to flare methane, as it is more environmentally and economically friendly. In 2012, these practices led to over \$1 Billion lost in fuel. A recent breakthrough involving the use of hydrogen peroxide (H_2O_2) in the partial oxidation of methane to liquid chemicals at ambient conditions has been made. This process, used an iron based zeolite catalyst, and moderate concentrations of peroxide. Although peroxide is produced inexpensively industrially, there are cost and safety concerns with shipping the product to the remote fields where it would be used in this process. Nitrogen doped carbon materials have been identified as promising electrocatalysts for the oxygen reduction reaction (ORR).

Here, the synthesis and subsequent testing of a NDC catalyst is reported. KIT-6, a mesoporous silica was used as a hard template, with an ionic liquid being the carbon and nitrogen precursor. Powder x-ray diffraction, N_2 adsorption, scanning electron microscopy, and elemental analysis were used to characterize the template and resulting catalyst. Pore size distribution of KIT-6 can be influenced by slight changes in the synthesis procedure. This was utilized in an attempt to change the

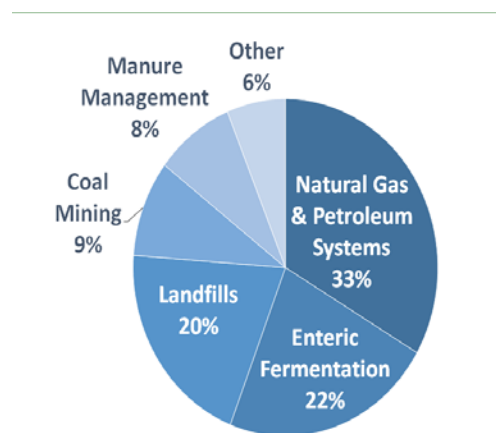
properties of the final catalyst. Slight changes in the hydrothermal ageing temperature changed the pore distribution in template, and the ECSA was significantly increased as a result. Rotating Disk Electrode (RDE) testing shows that the catalysts have high selectivity (90%) towards H₂O₂. A RDE is not a production method that can be used industrially. In the best circumstances, it would take over 4 hours to accumulate the required amount of H₂O₂ used by Hammond *et al.* Mass transport of the reactants to the surface of the catalyst hinders the overall activity. A flow cell type device can help overcome these limitations by delivering the reactants directly to the catalyst surface. Current densities of 50 mA cm⁻² with selectivity around 60% was achieved in the tested flow cell. This device would require ~40 minutes to produce the necessary amount of peroxide to be used if scaled up to 25 cm².

Chapter 1

INTRODUCTION

1.1 Methane Activation

Methane (CH₄) is a plentiful, naturally occurring hydrocarbon, and the main constituent of natural gas¹⁻⁴. Due to its abundance, it has been well studied as both a feedstock for chemical production and as a fuel⁵⁻⁶. Methane has become the subject of research as of late because it is often released into the atmosphere as a result of human activities such as: coal mining, natural gas or petroleum drilling, and breakdown of garbage in landfills⁷⁻⁸. As seen in Figure 1.1 these human activities account for over 60% of all methane emissions into the atmosphere. The highest percentage of



U.S. Environmental Protection Agency (2014).
U.S. Greenhouse Gas Inventory Report: 1990-2014.

Figure 1.1: U.S. Methane Emissions, by source, 2014⁸

emissions come from oil and natural gas sites, which account for 33% of all US methane emissions. Globally, methane emissions have been increasing over the past 20 years⁹. Figure 1.2 shows emissions by source that resulted from human actions. It can be seen that emissions rose by 25% between 1990 and 2010, with expected emissions rising another 22% by 2030.

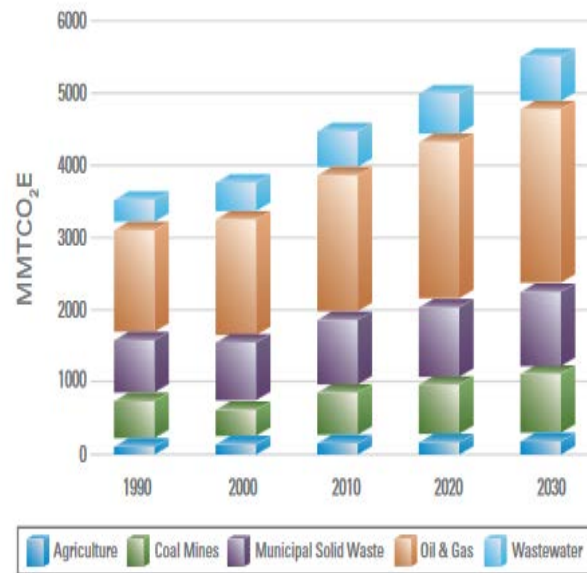
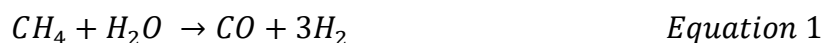


Figure 1.2: World Anthropogenic Methane Emissions⁹

Recently, oil companies have begun flaring off methane gas⁷. Flaring the methane is more environmentally friendly than venting the gas straight to the atmosphere because carbon dioxide, the main product of methane combustion has a greenhouse gas (GHG) potential 25x smaller than that of methane¹⁰. Flaring has become such a widespread practice in North Dakota that 1.4 billion cubic meters of natural gas were flared off during 2011. This number increased in 2012 leading to the release of 1 million cars-

equivalent of GHG, and over \$1 billion of fuel lost¹¹⁻¹². Despite how valuable this fuel can be, companies are simply flaring it off instead of capturing it and either selling it or using it. This ‘waste’ is due to the economics of the gas. In many situations, it is neither economical to use methane collected at a remote oil field as a raw material nor as a fuel. The cost to capture, compress, and ship methane to a chemical facility or distribution center or even burn it as a fuel at the remote field outweighs the benefits from using it as a raw material³.

Traditionally, methane has been used both as a fuel, and as the primary gas in steam reforming, a process used to produce Syngas, a mixture of carbon monoxide and hydrogen.¹³



Syngas is then be used in the synthesis of other chemicals, including methanol.

Methanol is produced via the hydrogenation of carbon monoxide.¹⁴



Methanol is mainly used as a feedstock chemical, meaning it is the starting chemical for the production of hundreds of other chemicals including acetic acid and formaldehyde. Methanol has many other uses, including use as a transportation fuel, laboratory solvent, and as an additive for water purification.¹⁵

The industrial process to produce methanol is very inefficient. Syngas production, the first step, is a very energy intensive process, occurring at high temperatures (~650°C). Another inefficiency in the process is the overcomplicated chemical pathway. Methane, which has carbon in the -4 oxidation state, is oxidized to

carbon monoxide which has carbon in the +2 oxidation state, and then reduced other compounds with a lower oxidation state of carbon. It would be advantageous to find a direct route from methane to these final products. Partial oxidation of methane at mild temperatures could solve both the previously mentioned disadvantages. Mild temperatures would reduce energy usage, while partial oxidation could directly produce the products needed, eliminating an unnecessary reduction step.

1.2 Partial Oxidation of Methane

The previously described method of oxidizing methane with the final product of methanol initially requires full oxidation of methane. Many valuable products, such as formic acid, formaldehyde, and methanol could be instead be created by partial oxidation of methane. Theoretically, partial oxidation of methane to these products would require less energy to produce, than would be required by the previously mentioned process of steam reforming and hydrogenation. This process, however, is the only option that is commercially viable today. This is due two to main factors. One key factor is the high C-H bond energy, >100 kCal/mol, it is the highest bond energy between carbon and hydrogen among hydrocarbons². This high bond energy gives methane great stability. The second factor is the ease at which methane can be overoxidized. Once, the C-H bond is broken, and oxidation begins, it is difficult to stop before CO or CO₂ are produced.

Recently, progress has been made partially oxidizing methane at mild conditions (50 °C). An iron based zeolite catalyst has been used in the presence of

hydrogen peroxide in this reaction¹⁶⁻¹⁷. It has been proposed that the zeolite based catalyst activates hydrogen peroxide, forming a hydroperoxy species that is able to cleave the C-H bond. The proposed mechanism is shown in Figure 1.3. Major products of this chemical oxidation include methanol and acetic acid. In the first step, one hydrogen atom in an $-OH_2$ group is replaced by $-OH$, forming $-OHOH$. This unstable intermediate breaks down forming $-OOH$, while a hydrogen atom is shifted onto another $-OH$ group, forming $-OH_2$. Peroxide attacks again, releasing H_2 , moving the $-OH_2$ and $-OH$ groups, and leaving oxygen double bonded to iron. The hydroperoxy species, $-OOH$, cleaves the C-H bond in methane, forming a $O-OH-CH_3$ while the hydrogen removes the double bond. Peroxide attacks for a third time, removing CH_3OOH , which can decompose into methanol and the catalyst system returns to step 2.

The catalyst presented by Hammond *et al.* has two main parts, the first part is the iron based ZSM-5. The second part is the copper ions that are introduced with the catalyst. Through a series of experiments, it was determined that Fe, which was integrated into the pore structure, was an integral part for the activation of hydrogen peroxide. The structure, seen below in Figure 1.3, was determined using a combination of EXAFS and DFT. The structure was consistent with previous reports of di-iron species within zeolites. DFT experiments were then used to further study the species within the framework. Based on DFT models and experimental data, Hammond *et al.* proposed that methyl hydroperoxide (CH_3OOH) was the primary product of the oxidation. Other products, methanol, acetic acid, and carbon dioxide,

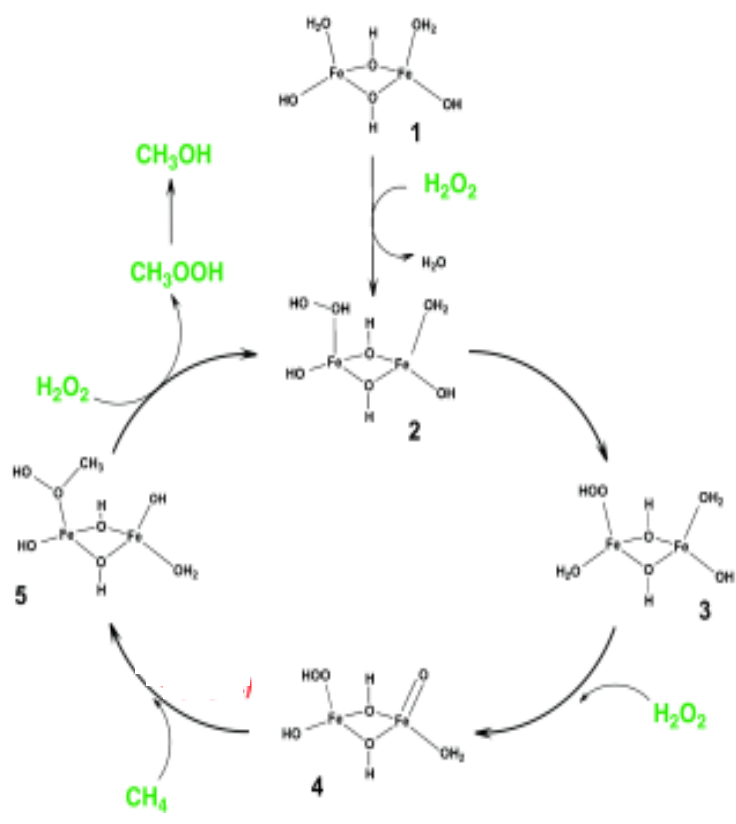


Figure 1.3: Catalytic cycle for the oxidation of Methane using Hydrogen Peroxide¹⁶

are formed consecutively after. The chemistry observed in this system is fundamentally different from the chemistry seen in Fenton's reagent. Fenton's reagent relies upon methyl radicals as an essential species in the mechanism. EPR spectroscopy revealed a distinct lack of methyl radicals, and therefore, is in agreement with the proposed mechanism. The proposed mechanism is of significance due to the high selectivity towards oxygenate species while Fenton's chemistry shows low selectivity towards these species.

The addition of Cu^{2+} is of importance because it limits the over-oxidation of methanol to other species. It is proposed that methyl hydroperoxide undergoes a surfaces catalyzed reaction that produces methanol and hydroxyl radicals. It is these radicals that react with methanol, forming formic acid and other species. Experiments show that Cu^{2+} is effective as either be part of the catalyst or as an additive to the system. Cu^{2+} does not impact methane oxidation activity, as overall conversion in the system was unchanged with its addition.

The system used in these experiments is one that would not be useful in an industrial setting. A small (< 25 mL) autoclave reactor was used. Because the reaction takes place between a liquid and a dissolved gas, activity and conversion are highly dependent on solubility of gas in the liquid. The system could theoretically be improved by making use of a packed-bed reactor, or any other such reactor where there are increased gas-solid-liquid interactions.

1.3 Hydrogen Peroxide

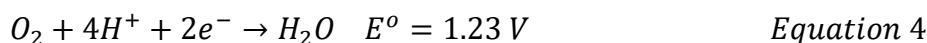
Traditionally produced by the anthraquinone process, hydrogen peroxide is one of the 100 most important chemicals in the world¹⁸⁻¹⁹. Hydrogen Peroxide is of interest due to its large volume of uses throughout many industries. It has been widely used in the bleaching of paper pulp, in the treatment of wastewater, as a household disinfectant, and in the destruction of organics²⁰⁻²³. It is environmentally friendly as it breaks down to Hydrogen and Oxygen, and as part of Fenton's Reagent, the reaction between it and Fe^{2+} can be used in acidic conditions to break down organic

molecules²⁴⁻²⁵. The traditional anthraquinone process is a batch process that requires hydrogenation and oxidation of anthraquinone molecules followed by separation of H₂O₂ from organics. This multistep process is very energy intensive, and requires the use of expensive catalysts. These factors make it difficult for on site or *in-situ* production, which could considerably lower costs in addition to allowing for optimization with the final application²⁶.

In-situ production of hydrogen peroxide would be very useful in a methane partial oxidation system. As discussed previously, there are high costs, and many hazards with shipping hydrogen peroxide long distances.

Electrochemical production of hydrogen peroxide has been suggested as an alternative to the anthraquinone process. Electrochemical reduction of oxygen to hydrogen peroxide is desirable because it could be a decentralized process that occurs at moderate temperatures and pressures²⁷. In addition to this, the energy required could be provided by green, renewable sources, such as wind or solar power.

Oxygen can undergo two separate reduction reactions²⁸. These reactions can be seen below, along with the standard thermodynamic potential, in Equations 3 and 4.



The thermodynamic potential is analogous to activation energy seen in traditional chemical reaction studies. For reduction, the reaction cannot occur unless the potential on the cathode is below the thermodynamic potential. The opposite is true for oxidation reactions: the reaction will not occur on the anode unless the potential is

above the thermodynamic potential. Just like in traditional reaction chemistry, more energy is usually applied to boost reaction kinetics. Some product should be seen if the minimum activation energy is applied, however the rate of production will likely be negligible. In electrocatalysis the extra energy needed is called overpotential (η). Overpotential is used as a means of comparing catalysts for the same reaction. Theoretically, at a very small overpotential (0.01 V), the desired reaction will occur. In practicality, there are many other things that affect the desired reaction. At such a small overpotential, there is high likelihood of negligible reaction kinetics. In addition to this, there might be side reactions occurring that are more favorable at the conditions. For H_2O_2 production via electrochemical methods, a cheap catalyst, which is highly active and highly selective to 2-electron reduction of oxygen at low overpotential, is needed.

Recently, many electrocatalysts for H_2O_2 have been discovered and tested. Many of these catalysts include metals such as Au, Pd, Co, Hg, and Pt²⁹⁻³⁶. Although some of these materials have been shown to be highly selective (70-90%) towards H_2O_2 , the cost and limited supply restricts the potential application going forward.

Recently, a Pt promoted Pd/Au nanoalloy has shown promise in the direct synthesis of H_2O_2 from H_2 and O_2 , developed by Edwards *et al*³⁷. Bimetallic and trimetallic combinations of Au, Pd, and Pt were used in experiments with total metal composition kept at 5%. A 2.28:2.28:0.45 combination of Au:Pt:Pd was determined to be ideal, however that combination is also very active for the hydrogenation reaction of H_2O_2 to H_2O . The best overall performance, including the hydrogenation reaction

was a 2.4:2.4:0.2 mixture. This catalyst is able to produce $170 \text{ mol kg}_{\text{cat}}^{-1} \text{ hr}^{-1}$.

Experiments for this catalyst were carried out in an autoclave type reactor, used CH_3OH as a solvent and H_2/CO_2 as well as O_2/CO_2 .

The ideal electrocatalyst would be comprised of abundant, non-metal elements. Carbon based materials could be a promising alternative to metal based catalysts, as carbon is a highly abundant, inexpensive material. Many carbon materials such as graphite and porous nitrogen doped carbon have been shown to be active catalysts for H_2O_2 electroproduction. Recently, these materials have reached selectivities of 90% or more³⁸⁻⁴⁵.

One such carbon-based catalyst that shows promise for the ORR reaction was reported by Fellingner *et al*³⁹. This catalyst was prepared using the nanocasting technique⁴⁶. Commercial silica particles were used as the hard template while an ionic liquid was used as the precursor dopant. The catalyst was made by calcining the template and precursor at high temperatures, and subsequently removing the hard template. The catalyst was deposited onto a glassy carbon electrode and tested using a Rotating disk electrode (RDE) system. Experiments to determine both activity and selectivity were conducted. Using LSV, the activity at various potentials was measured, and compared to other catalysts of a similar nature. Koutecky-Levich analysis the selectivity towards H_2O_2 was determined to be in the low 90% range. Although this is not an extraordinary result, Hasché *et al.* did show that activity significantly increased when the catalyst was used in a neutral electrolyte⁴⁰. The source of the activity lies in the bonded N atoms. Graphitic, pyridinic, and pyrrolic

nitrogen are present in the catalyst. The presence of nitrogen in these forms changes the electronic properties of the catalyst. This increases the activity compared to a pure carbon catalyst. Nitrogen content was determined to be about 17%.

Another Nitrogen doped carbon catalyst, synthesized in a similar fashion, had similar performance slightly higher selectivity. This catalyst, developed by Park *et al*⁴⁴, used a nitrogen containing organic compound, and a different silica source, KIT-6 as the hard template. Park performed many of the same experiments that Felliger *et al.* performed, and overall, the catalyst was better. Despite the moderate drop in activity (~30%), the selectivity improved to over 93%. Park tested two separate types of nitrogen doped carbon catalysts, one derived from a hard template, and the other derived solely on the precursor. The hard template derived catalyst significantly outperformed the other catalyst. Park theorized that the larger pores diameter in the hard-template derived catalyst allowed for better mass transport in and out of the pore, reducing the opportunity for 4-electron reduction of O₂.

The nitrogen doped carbon catalyst has many advantages over the Au:Pd:Pt trimetallic catalyst. The electrocatalyst is made from inexpensive materials, while the trimetallic is made from expensive precious metals. In addition, hydrogenation reactions are non-existent on the carbon catalyst, as there is little to no hydrogen gas in the electrolyte. Furthermore, the ability to change potentials allows for control over reaction rate and activity. This is not possible in the trimetallic system.

Ideally, the two separate reaction systems, the oxygen reduction and methane oxidation, could be integrated into one comprehensive system. The first part of the

system would be electrochemical oxygen reduction. The products would be fed into a reactor, where methane partial oxidation would occur. Although methane oxidation has only been tested on a batch scale, research can be done to prove the system on a continuous scale.

Chapter 2

METHODS

2.1 Preparation of KIT-6

The procedure for the preparation of mesoporous silica KIT-6 was reported by Rosen⁴⁷ *et al* and Kleitz *et al*⁴⁸. In a typical synthesis, 10 g of tri-block copolymer P123 (Sigma-Aldrich) was dissolved in an aqueous solution containing 375 mL of deionized H₂O (≥ 1 M Ω , Barnstead, Thermo Fisher) and 17 mL of HCl (Sigma Aldrich, 37wt%). The solution was heated to 34°C and 10 g of 1-butanol (Fisher Chemicals, Certified ACS) was added and the mixture was stirred vigorously at 34°C for at least one hour. Then, 21 g of tetraethyl orthosilicate (Alfa Aesar, 98%) was added and the mixture was stirred for 24 hours at 34°C. The resulted mixture was transferred into Teflon autoclaves, sealed, and maintained at either 80°C, 100°C, or 120°C for another 24 hours. After the thermal treatment, the mixture was filtered and treated with a mixture of 20 mL of HCl and 200 mL of ethanol (Deacon Labs, 200 Proof), and washed with DI water. The resulting powder was calcinated in air at 550°C for 3 hours to remove the polymer template.

2.2 Preparation of Nitrogen Doped Carbon Catalyst

The procedure for the preparation of the Nitrogen Doped Carbon Catalyst was based off of a procedure reported by Fellingner *et al*³⁹. In a typical synthesis, 1g of

KIT-6 was mixed with 3g of 1-Ethyl-3-methylimidazolium dicyanamide (Sigma-Aldrich, 98%) and 10g of EtOH. The mixture was stirred for 1 hour, and dried in air at 90°C for 1.5 hours, until a paste-like consistency was achieved. The mixture was then calcined under Nitrogen at 800°C in the following manner. First, nitrogen was used to purge the space for 1 hour. Then, the mixture was calcined at 800°C for 2 hours with a 10°C/min ramp. The resulting powder was left to cool overnight. The silica template was removed from the resulting black powder by stirring for 1 hour in 3M NaOH solution. The NaOH solution was consisted of NaOH (Fisher Chemicals, 95%) in 50/50 mixture of EtOH and H₂O. The final NDC powder was recovered using centrifugation. The supernatant was decanted, and the powder was washed with 50/50 H₂O and EtOH a total of 3 times. The powder was left to dry overnight at 60°C.

2.3 Electrochemical Testing

2.3.1 Rotating Disk Electrode

Electrochemical testing was carried out using cyclic voltammetry (CV), linear sweep voltammetry (LSV) and chronoamperometry, in both a RDE system and flow-reactor system. For the RDE system, 10 mg of NDC was sonicated in 1.99 mL of H₂O, 0.5 mL 2-Propanol (Fisher Scientific, Certified ACS), 10 µL Nafion Ionomer Solution (Sigma-Aldrich). 15 µL of the previous solution was dropcasted onto a 5 mm OD glassy carbon (GC) electrode (Pine). The solution was dried on a pre-polished GC electrode for 15min at 60°C. Polishing was done with 0.05 µm alumina solution using an Eco-Met 250 (Buehler)

In order to evaluate the catalytic performance, a Princeton Applied Research VMP2 potentiostat was used with a 3 electrode RDE setup. RPM was controlled by a MSR-X control box (Pine). The counter electrode was a graphite rod. The electrolyte was 0.5M Na₂SO₄ (Sigma-Aldrich, ACS). Current was measured against a Ag/AgCl reference electrode (Pine) and converted to the reversible hydrogen electrode (RHE) Scale.

CV and LSV scans were the first technique used to observe onset potential and activity of the NDC. The scan rate was 5 mV/sec. CV scans were done in both oxygen and nitrogen rich electrolyte and the nitrogen current was subtracted from the oxygen current to eliminate background capacitive effects.

2.3.2 Koutecky-Levich Plots

Koutecky-Levich plots were generated to determine selectivity of the NDC towards H₂O₂. These were done at different potentials by varying the spin RPM at different potentials and taking the average of multiple data points. Rotation speeds were 400, 900, 1600, and 2500 RPM. Data is plotted as 1/j (cm²/mA) vs $\omega^{-1/2}$ (sec^{1/2}). The plotted data is linear, and the selectivity can be determined based on the slope. The number of electrons transferred can be determined by using Equation 5.

$$\frac{1}{n} = 0.62 \cdot B \cdot F \cdot D_{O_2}^{\frac{2}{3}} \cdot \nu^{-\frac{1}{6}} \cdot C_{O_2} \quad \text{Equation 5}$$

n represents the number of electrons transferred, B is the best fit linear slope, F is Faraday constant, D is the diffusivity of oxygen in the electrolyte, Na₂SO₄, ν is the kinematic viscosity, and C is the bulk O₂ concentration. The number of electrons

transferred will be in-between 2 and 4. The closer the number is to two, the higher the selectivity is towards H₂O₂. Specifically, the selectivity can be obtained using Equation 6.

$$Selectivity = \left(2 - \frac{n}{2}\right) \cdot 100\% \quad \text{Equation 6}$$

Where n is the number of electrons transferred, found above in Equation 5.

2.3.3 Electrochemical Surface Area

Electrochemical Surface Area was determined based on the double layer capacitance (C_{DL}) of the NDC on GC electrodes in 0.5M Na₂SO₄⁴⁹. Capacitance was measured by recording anodic-cathodic currents (I_c) in a potential region void of faradaic processes. Scan rates were varied (ν) and the capacitance was determined using formula # below. A plot of I_c vs ν will be linear and have a slope of C_{DL} .

$$I_c = \nu \cdot C_{DL} \quad \text{Equation 7}$$

2.3.4 Micro Flow Cell

As previously mentioned, a micro flowcell reactor was used to test the NDC catalyst for an extended period of time⁵⁰. The basic geometry of the device can be seen below in Figure 2.1 The figure shown below is merely the base configuration, as changes were made based on experimentation. The same catalyst solution recipe was used between the RDE and Flow-Cell experiments. 75 μ L of solution was pipetted onto a 1 cm² carbon paper (Sigracet 35 BC, FuelCellStore) and dried in an 80°C oven. The exchange membrane was Nafion XL, which was pretreated in dilute acid before use. Both the catholyte and anolyte were 0.5 M Na₂SO₄. In all tests the anolyte was

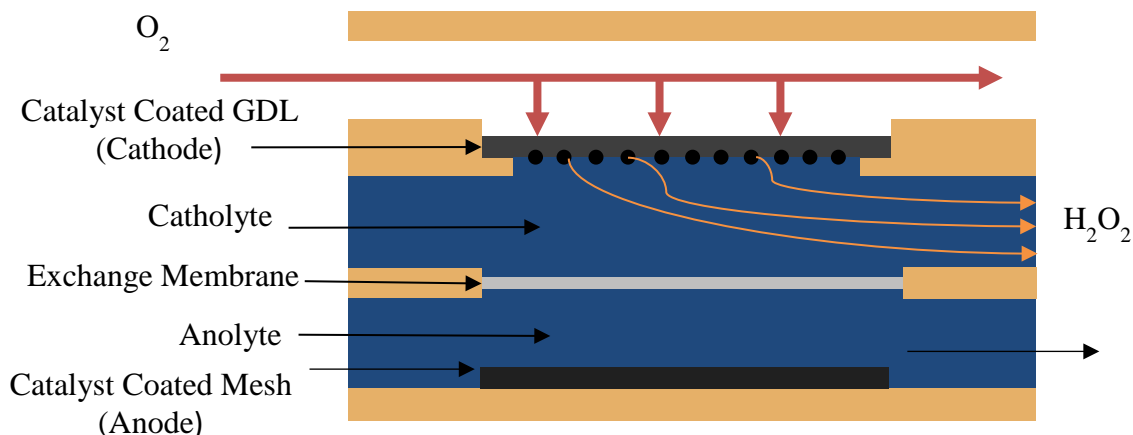


Figure 2.1: Micro Flow Cell Reactor

recycled for the duration of the experiment. The catholyte however, was not recycled. Concentration was determined using the potassium titanium (IV) oxalate method.

Ir-based catalysts on freestanding Ti-based supports were constructed via a dip coating and thermal decomposition method. Ti-Mesh was etched for 60 minutes in boiling 0.5M oxalic acid (Sigma-Aldrich, $\geq 98\%$). The mesh was dip coated in a solution of 10 mL isopropanol (Fisher Chemicals, ACS Reagent) 30 mg $\text{IrCl}_3 \cdot x\text{H}_2\text{O}$ (Alfa Aesar, 99.8%,) with 10% HCL (Fisher Chemicals, ACS Reagent). The mesh was dried at 100 °C for 10 min, and then calcined at 500 °C for 10 minutes. This process was repeated six times total. In other experiments, Ir was sprayed directly onto the Nafion exchange membrane. The solution consisted of 3 mL Isopronaol, 200 mg Ir Black (Premetek), 2.3 mL nafion ionomer and 5 mL distilled water.

2.3.5 Chronoamperometry Testing

Chronoamperometry tests were conducted to determine the concentration of H_2O_2 generated overtime and the stability of the catalyst. The same RDE setup

described above (CV scan) was used. A Cary 60 UV-VIS (Agilent Technology) was used to in conjunction with the potassium titanium dioxide method to determine peroxide concentrations over time.

2.3.6 Potassium Titanium (IV) Oxalate Concentration Method

The potassium titanium (IV) oxalate method is a photometric method that measures the absorbance of the a titanium(IV)-peroxide complex⁵¹. The intensity of absorption follows the beer-lambert law so the absorption is directly correlated to the peroxide concentration. In this method the titanium reagent was made using the following procedure: 272 mL of concentrated sulfuric acid (Fischer Chemicals, ACS+) was mixed with 35.4 g of potassium titanium(IV) oxide oxalate dehydrate (Sigma-Aldrich, $\geq 98\%$ Ti) and made up to 1L with distilled water. 5 mL of the titanium reagent and 5 mL of peroxide containing electrolyte was mixed and made up to 25 mL. A blank solution was made using the same procedure. The blank solution used 5 mL of peroxide free electrolyte. The absorbance was measured at 400nm for both the sample and blank. H_2O_2 concentration was determined using Equation 8

$$[H_2O_2] = \frac{A - A_b}{37.4 \cdot x \cdot l} \quad \text{Equation 8}$$

where x is the amount of peroxide solution per 25ml of total solution, l is the path length of the spectrophotometer cell in cm, and A and A_b are the absorbances at 400 nm for the peroxide solution and blank solutions respectively. All measurements were done using a Cary 60 UV Vis (Agilent Technologies).

2.4 Characterization Techniques

X-ray diffraction (XRD) measurements were conducted on a Bruker D8 X-ray diffractometer using Cu K α radiation.

Scanning electron microscopy (SEM) images were collected using a JEOL JSM-7400. The JEOL instrument had an EDS detector attached which was also used. Some samples were first sputter-coated to increase conductivity.

Elemental Analysis to determine the carbon, hydrogen, nitrogen and sulfur content of the NDC catalysts was performed using an Elementar vario EL cube.

N₂ adsorption experiments were performed using a Micrometrics 3Flex adsorption instrument, with appropriate sample degassing beforehand.

Chapter 3

NITROGEN DOPED CARBON CATALYST SYNTHESIS AND CHARACTERIZATION

3.1 Nitrogen Doped Carbon

As previously mentioned, Nitrogen Doped Carbons have been extensively studied for the ORR reaction to both water and hydrogen peroxide. The allure of these compounds is that they can be made from inexpensive, non-metal materials. In addition, they are relatively easy to make, even though the procedure spans many days. Many of these catalysts from literature are synthesized using the nanocasting technique.

3.2 Nanocasting

Mesoporous materials, such as silica, carbon, and alumina have long been used as a hard template in the synthesis of other materials⁵²⁻⁵³. These hard templates hold the mesoporous ordering while a second phase forms in and around the pores of the template material. After the new phase is formed, the template is removed through processes such as leeching or calcination. The second phase is left as an inverse of the original template. Figure 3.1 below depicts this process. To form the structure inside of the pores of the hard template, the precursors must be loaded into the pores. Generally, precursors must be dissolved into a solvent to ensure that the solution will interact with the hydrophilic surface of the silica. The most basic method, incipient

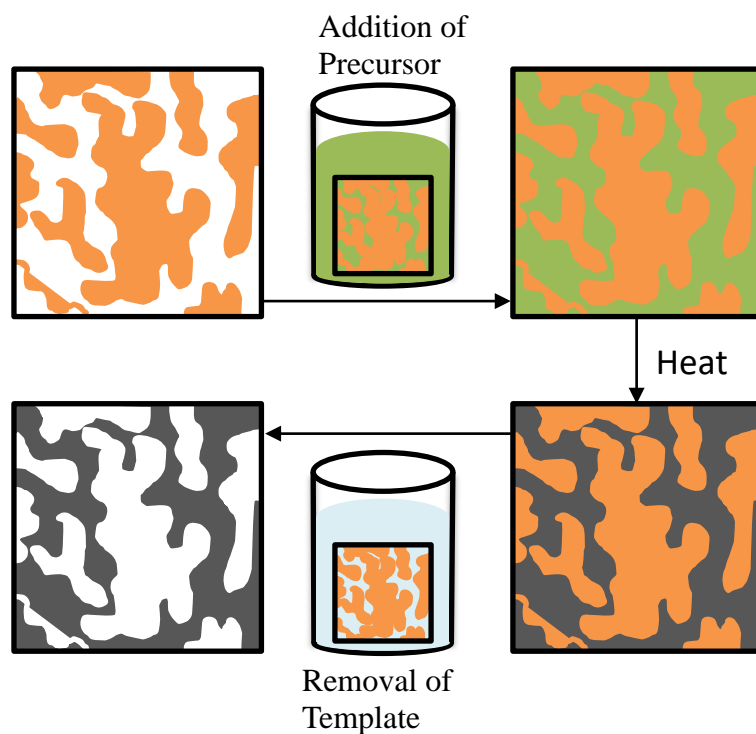


Figure 3.1: Nanocasting process

wetness, is a process where the precursor is dissolved into water or ethanol and the subsequent solution is dripped onto the hard template. Other methods such as suspending the template in a hydrophobic solution instead of a hydrophilic one, can be used. In this scenario, the hydrophilic precursor should be attracted to the hydrophilic silica, increasing the likelihood that the precursor will go into the pores of the template. Ideally, the precursor will fill the pores entirely, and therefore the final phase will have the same volume as the pores of the template. In practice, this rarely happens so alternative methods must be used to maximize the loading. One such technique is repeated impregnation and calcination. Here, the steps are repeated multiple times, allowing the second phase to completely fill the pore structure. Although this process

can be time consuming, it is helpful in ensuring that there is maximum yield from the hard template.

3.3 KIT-6

The first step in the creation of the catalyst, is the preparation of the hard template. KIT-6 was chosen as a hard template because studies have shown that pore size distribution can be altered through variation of the ageing temperature. This slight change could have an impact on the physical properties of the resulting material, as well as an impact on the catalytic properties of the catalyst.

3.3.1 Powder X-Ray Diffraction

Synthesized KIT-6 was characterized using PXRD. An example of one such sample can be seen below in Figure 3.2⁵⁴.

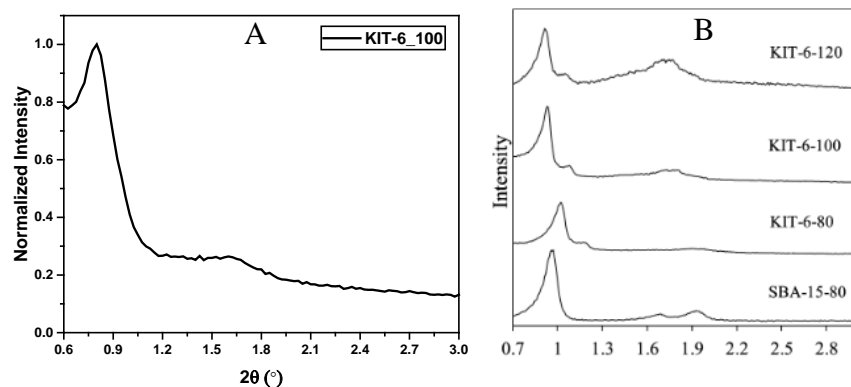


Figure 3.2: A) XRD diffractogram of KIT-6_100, B) Literature KIT-6 diffractogram used for comparison. Adapted with permission from Pirez, C.; Caderon, J.-M.; Dacquin, J.-P.; Lee, A. F.; Wilson, K., Tunable KIT-6 mesoporous sulfonic acid catalysts for fatty acid esterification. *ACS catalysis* **2012**, 2 (8), 1607-1614. Copyright 2012 American Chemical Society⁵⁴

It is clear from the diffraction pattern and the literature, that KIT-6 was successfully made. This is only one example of a typical sample. KIT-6 was synthesized many times, and characterized using PXRD. Each sample tested had a similar diffraction pattern, and therefore were not included here.

3.3.2 N₂ Adsorption

Gas adsorption is a powerful technique to probe the enhanced surface area and pore characteristics that porous and nanostructured materials possess. An inert gas (often N₂) is dosed over a sample that has been cooled by liquid N₂. Adsorption occurs on the surface of the material and for multiple layers above it. By measuring the pressure, the amount of adsorbed gas can easily be determined. The Brunauer-Emmett-Teller (BET) theory can be applied to find the surface area of the material. The Barrett-Joyner-Halenda (BJH) method can be used to characterize the pore sizes.

Figure 3.3 presents the N₂ adsorption isotherms and pore size distributions for both the silica as well as the NDC carbon material. Both the BET surface area of ~780

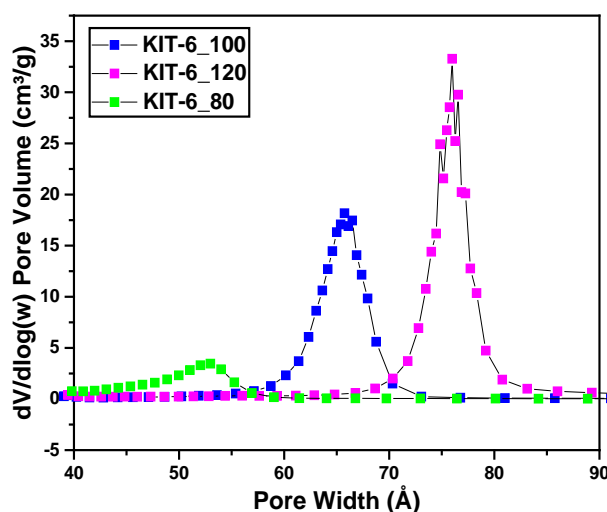


Figure 3.3: N₂ BJH Desorption pore size distribution of KIT-6

m^2/g and the pore size of around 6.5 nm for the silica that was aged at 100 °C are consistent with the literature. Silica particles aged at 120 °C and 80 °C, which have similar BET surface areas and pore sizes of 7.5 nm and 5.5 nm respectively, are also consistent with the literature.

3.4 Synthesized NDC Catalyst

3.4.1 N_2 Adsorption

Gas Adsorption was performed on the two catalysts that performed the best in RDE testing, NDC_80 and NDC_100. Pore size distributions can be seen below in Figure 3.4. Both catalysts have pore sizes centered around 3.6 nm. This corresponds to the wall thickness of the KIT-6 template. BET surface area for the catalysts was determined to be $699 \text{ m}^2 \text{ g}^{-1}$ and $716 \text{ m}^2 \text{ g}^{-1}$, with the larger value belonging to NDC_100

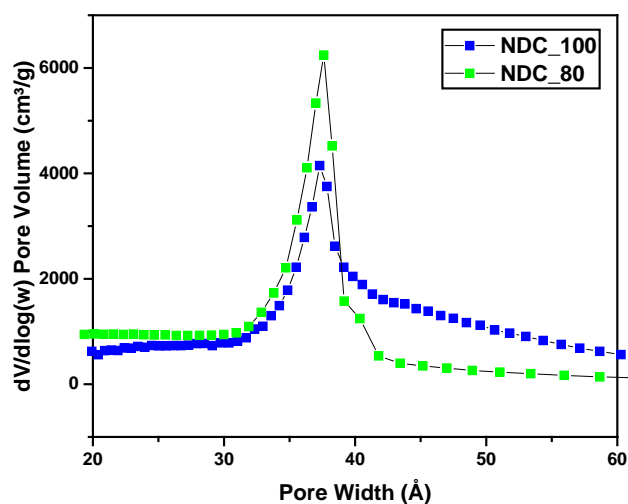


Figure 3.4: N_2 BJH Desorption pore size distribution of NDC Catalyst

3.4.2 SEM Micrographs

Example SEM micrographs can be seen below in Figure 3.5.

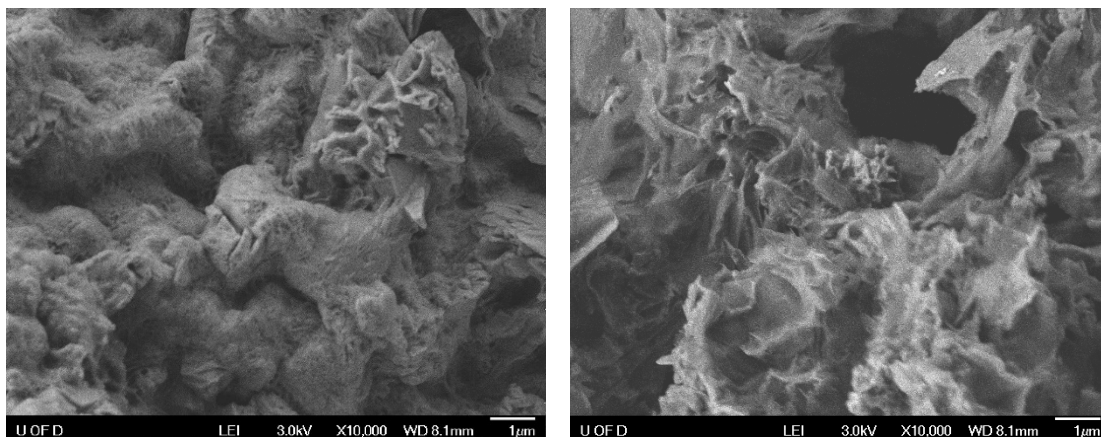


Figure 3.5: (A,B) SEM micrographs of synthesized NDC catalyst

Gas adsorption confirms that some properties of the template have been passed on to the final catalyst. However, these pictures paint a murkier picture. There isn't a clear uniform structure present in these SEM images, as would be expected. It is possible that TEM imaging is gain a better understanding of the structure.

3.4.3 Elemental Analysis

All three catalysts were tested to determine the carbon/nitrogen ratio.

NDC_120 and NDC_100 had very similar C/N ratios of 3.35 and 3.73 respectively.

NDC_80 had a much larger C/N ratio of 7.71.

3.4.4 Electrochemical Surface Area / Double Layer Capacitance

Double layer capacitance measurements were done using the aforementioned RDE set-up. However, there was no rotation of the electrode. First, CV scans at varying scan rates between 5 and 200 mV/s were completed in a non-faradaic area. Plots of the

current vs. scan rate were linear in nature, and the slope is equal to the double layer capacitance. The capacitance is directly proportional to the electrochemical surface area. Results from testing can be seen below in Figure 3.6. It can clearly be seen that as the calcination temperature increases, the capacitance decreases. The slope for NDC_80 is much larger than NDC_100 or NDC_120. As the calcination temperature of the KIT-6 increases, pore size also decreases.

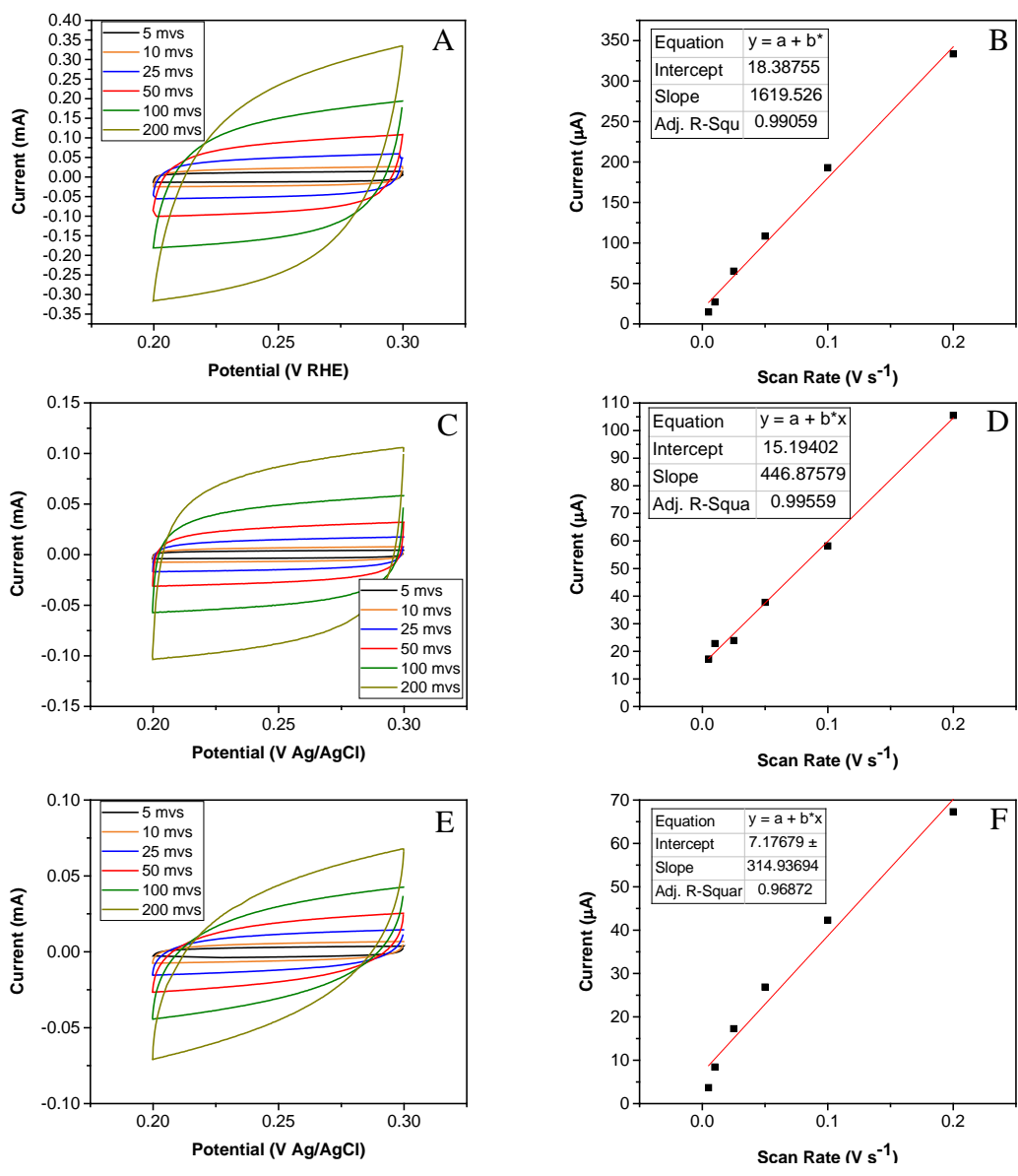


Figure 3.6: (A,C,E) CV scans in non-faradaic area of ORR Reaction for NDC_80, NDC_100, and NDC_120, (B,D,F) Linearized plots to determine double layer capacitance

Chapter 4

OXYGEN REDUCTION REACTION EXPERIMENTS

4.1 Oxygen Reduction Reaction

Electrochemical oxygen reduction reaction has two products, H_2O_2 and H_2O . Hydrogen peroxide is formed through 2-electron reduction while water is formed through 4-electron reduction. In this case, peroxide is the desired product while water is the unwanted product. There are two main factors that affect the amount of product that can be produced. Those factors are selectivity and current. There are virtually an unlimited number of current/selectivity combinations that would result in the production of a desired amount of product. A very high current coupled with a low selectivity could produce the same amount of product as a low current coupled with high selectivity. In this case, it is more important that the catalyst is highly selective towards hydrogen peroxide production, even if the selectivity comes at the expense of total activity. Peroxide is needed in high concentrations downstream and lower selectivity would dilute that stream. If the separation process between peroxide and water was very cost effective, and straightforward, a higher peroxide production might be desired compared to a high selectivity.

4.2 Rotating Disk Electrode

The NDC Catalysts tested were made from 3 different KIT-6 materials. One silica template was calcined at 80 °C, one at 100 °C, the last at 120 °C. Results from LSV

scans are shown below in Figure 4.1. There are a couple of important pieces of information contained within the scan. They are the onset potential, and the total current density. The onset potential is the potential where faradaic activity begins to take place. This is important, because it gives us the minimum over potential needed to drive the reaction. Overpotential is generally related to energy efficiency. The closer the potential is to the thermodynamic potential, the less energy is being used to drive the reaction.

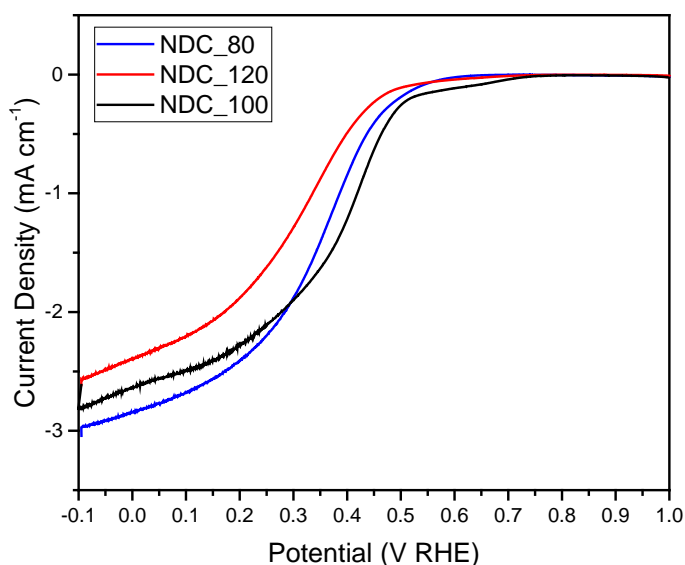


Figure 4.1: LSV Scan of NDC_80, NDC_100, and NDC_120

Three scans are shown in Figure 4.1. Onset potential is the lowest for NDC_100 followed by NDC_80 and NDC_120. Based on onset potential we know that oxygen is being reduced with less of an energy penalty. This is good from a theoretical standpoint, but activity is still important when looking at the electrochemical activity as a whole. Total electrochemical activity is the other

important information that can be obtained from the graph. It is clearly shown that the activity for NDC_120 is the poorest, as the current density is the smallest throughout the entire potential range tested. It is not clear from the scan if NDC_80 is better than, equal to, or worse than, NDC_100. Although the total absolute current is higher at potentials less than 0.3 V RHE for NDC_100, meaning that in general, more products were being created, it remains to be seen how the amount of peroxide being created at those potentials relates to the total amount of product. Although the onset potential is lower in NDC_80 than it is in NDC_100, the current is likely too small at these potentials to see any appreciable production of products. Therefore, it will be more important to look at more negative potentials for peroxide production.

At lower potentials (< 0.3 V RHE), the total current is largest for NDC_80. NDC_80 also had the largest ECSA, followed by NDC_100 and NDC_120. A connection can be made between the activity and ECSA. As the ECSA increases, so does activity below 0.3 V RHE. The electrochemical surface area followed the trend of template pore size. The smaller the pore, the larger the ECSA.

BET surface area and BJH desorption pore sizes were very similar for NDC_80 and NDC_100. It is likely that they had no effect on the performance of the catalysts. Based on this, it is likely that the differences in ECSA result from another difference in the catalysts. Further studies would have to be conducted to determine the cause.

4.2.1 Koutecky-Levich

As previously mentioned, selectivity is very important to understanding the electrochemical properties of the catalyst. Selectivity was looked at only for the two most promising catalysts, NDC_80 and NDC_100. Koutecky-Levich plots for these two catalysts are shown below in Figure 4.2. Based on the Levich equation, a larger slope equates to a higher H_2O_2 selectivity. Across the 7 potentials shown, there is little difference in the selectivity of NDC_80. There is a clear difference between the selectivity at 0.3 V RHE and 0.0 V RHE. The selectivity actually decreases when moving towards higher overpotentials. The selectivity for each potential can be seen below in Table 4.1.

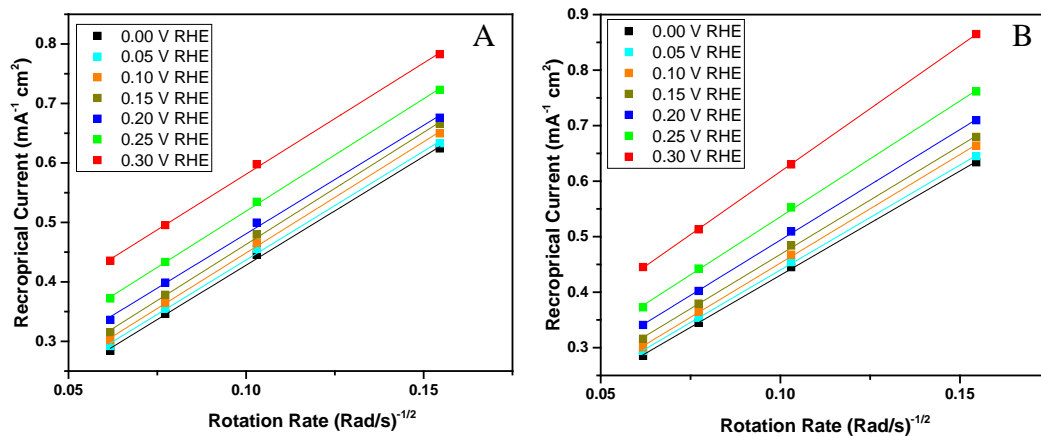


Figure 4.2: Koutecky-Levich plots at various potentials for A) NDC_80 and B) NDC_100

The selectivity is very close to 84% H_2O_2 for all the potentials tested on NDC_80.

This catalyst is surprisingly stable over the wide range of potentials tested. The other

Table 4.1: Selectivity of NDC_80 and NDC_100

Potential (V vs. RHE)	Selectivity (%)	
	NDC_80	NDC_100
0	83.0	78.3
0.05	84.6	79.2
0.1	85.0	83.1
0.15	85.2	83.3
0.2	84.8	85.3
0.25	84.3	90.5
0.3	83.8	99.2

catalyst, NDC_100 has selectivities ranging from 78% to 99%. As expected based on the Levich plot, the highest selectivity is seen at the lower overpotential (0.3 V RHE). Due to mass transport limitations this trend is expected. As the overpotential increases, the rate of reaction increases. However, the rate of transport of reactants to the catalyst surface does not increase. These things combined lead to the over-reduction of the products, producing more H₂O and less H₂O₂. The 99% selectivity seen in NDC_100 is among the highest seen in the literature. However, the significant drop off is disappointing. Many other NDC catalysts have stable stabilities in the low 90% for the same potential range as tested here. Based on these other catalysts 85% selectivity is disappointing. It is a good sign that it is at least stable, and should provide good partial current densities at higher overpotentials.

4.2.2 Partial Current Densities

Partial current densities are shown along with total current densities in Figure 4.3.

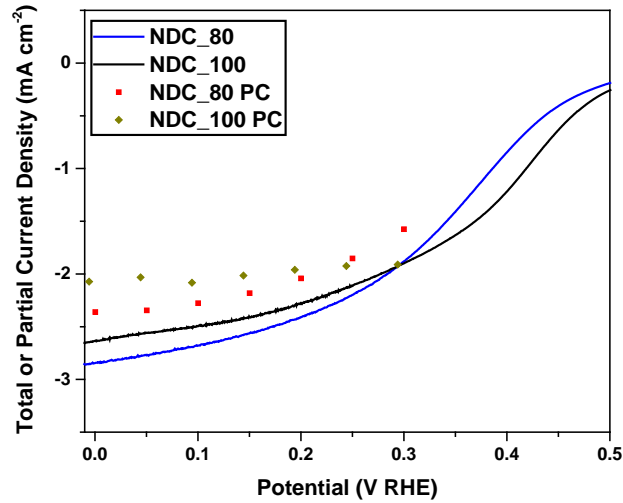


Figure 4.3: Total and partial current density of NDC_80 and NDC_100

As expected based on the total current density and higher selectivity at the higher overpotentials, the H_2O_2 partial current density is higher for NDC_80 than it is for NDC_100. This is true for most of the range of potentials tested. The partial current density remains this way until 0.25 V RHE where NDC_100 has better performance. Since the ultimate goal is to produce hydrogen peroxide for methane oxidation it is necessary to produce enough H_2O_2 to meet the requirements of the experiments performed by Hammond *et al.* Production rate in electrochemistry can be determined using Equation 9, seen below.

$$Q = nFN \quad \text{Equation 9}$$

Where Q is the total charge passed, n is the number of electrons transferred, F is Faraday's constant, and N is the moles produced. This equation can be substituted with Equation 10 to find the production rate

$$I = nF\dot{N} \quad \text{Equation 10}$$

In this equation, I is the current while \dot{N} is the rate of production in mol/s

Using this formula, and assuming 25 cm^2 it can be seen that the more productive catalyst at 0.3 V RHE , NDC_100, would require over 5.5 hours to produce enough peroxide to be used in the experiments of Hammond *et al.*. Looking at the highest overpotential, 0.0 V RHE , the better catalyst in this case, NDC_80, would take just over 4 hours to produce enough peroxide to be used in the experiments.

It is well known that increasing the rotation speed will increase the current, and therefore the amount of products produced. This can be seen in Figure 4.4 below. As the rotation speed increases, the total current increases. From 1600 to 2500 RPM the current increases by about 25%. A rotating disk electrode is not an ideal nor practical method to produce a product via electrochemical means. A more practical method would involve the use of a flow cell. Flow-cells or electrolyzers are more practical because they can increase the amount of reactants at the surface thereby increasing current and product production.

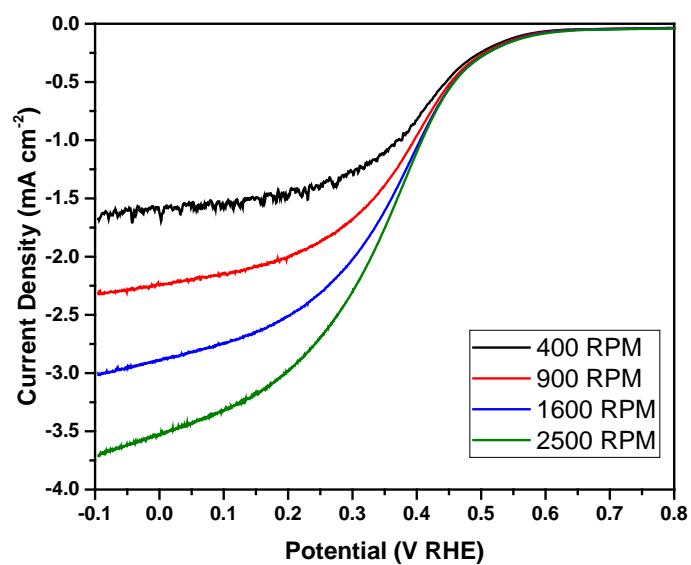


Figure 4.4: Typical plot of current vs potential at varying rotation speeds

Chapter 5

MICRO FLOW CELL

5.1 Design

A flow cell is the best method to increase the rate of H_2O_2 ⁵⁵. It was clearly shown that the current increased in the RDE cell as the rotation speed increased, and therefore, the mass transport of reactants to the catalyst surface increases as well. A well designed flow cell will ensure that mass transport limitations have been eliminated. When designing the flow cell, there are many things that need to be taken into consideration. A robust material, that will not interfere with the reaction, and that will not degrade over time is needed. Resistance is another factor to consider in electrochemistry. Generally, resistance is highest in three places throughout the cell. There is resistance between the cathode and membrane, across the membrane itself, and between the membrane and anode. It is advantageous to limit the resistance as much as possible. Equation 11 shows the relationship between voltage, current, and resistance.

$$V = I \cdot R \qquad \text{Equation 11}$$

Where V is the voltage, I is current, and R is the resistance. Based on this equation, when Voltage is held constant current decreases as resistance increases. Another way to look at this is by holding current constant. When current is held constant, a higher

resistance results in a higher voltage. This in turn results in a higher overpotential, and a lower energy efficiency. One way of reducing the resistance, is by increasing the concentration of the electrolyte. This will only work up to a certain concentration and the resistance will eventually level off. Another way of decreasing the resistance is by decreasing the physical distance between the electrodes and the membrane. If there is less material in-between the membrane and electrodes, resistance will be lower. There is no way of decreasing membrane resistance with the exception of changing the membrane, or removing it. Removing the membrane is not feasible as there would be inherit risk of reduction products crossing over to the anode and being oxidized. Another design factor to consider is how the reactants will be fed to the surface of the catalyst. Ensuring that there are large amounts of reactants present at the surface is important.

With these considerations in mind, a cell was designed based on the literature. A schematic is shown in Figure 2.1, and a picture is shown in Figure 5.1.



Figure 5.1: Constructed flow cell

The chosen material is cast acrylic. This is both transparent, and is resistant to peroxide as well as sodium sulfate. The individual channels are only 1.5 mm thick. This will help reduce the resistance in the cell, limiting extra energy wasted.

In the cell, the gas compartment is the furthest to the top followed by the cathode compartment and then the anode compartment. The gas is on top to reduce the chances of flooding the catalyst. Ideally the gas and liquid meet at the surface of the catalyst. These three things occurring at the same place are needed for the reaction to occur. If the electrolyte is flooding the catalyst/electrode it will be hard for the gas reactants to reach the electrode surface and react. Not pictured is the external reference electrode. From RDE studies we know the selectivities at different potentials compared to RHE. Although not practical in an industrial setting, a reference electrode is needed in these tests to determine the cell potential at various potentials compared to RHE on the cathode.

Initial flowcell testing was carried out using a graphite plate as the anode. A graphite rod was used in the RDE cell, and no adverse effects were seen. However, the current density was much higher in initial flowcell testing. Currents reached upwards of 80 mA in these tests. This high current led to an oxidation of the graphite electrode, seen in Figure 5.2. There was a clear indentation seen in the dark spot, arising from the oxidation of the material. Due to this material degradation, another anode catalyst was considered.



Figure 5.2: Oxidized graphite electrode

5.2 Initial Testing

Based on literature, Iridium Oxide was chosen to be a suitable catalyst for the water electrolysis reaction happening on the anode⁵⁶. Iridium oxide is a very stable and active catalyst for this reaction. Initially, Ir on Ti-mesh was used as the anode catalyst. There was no noticeable catalyst degradation compared to the graphite electrode. An example of a typical test is seen below in Figure 5.3

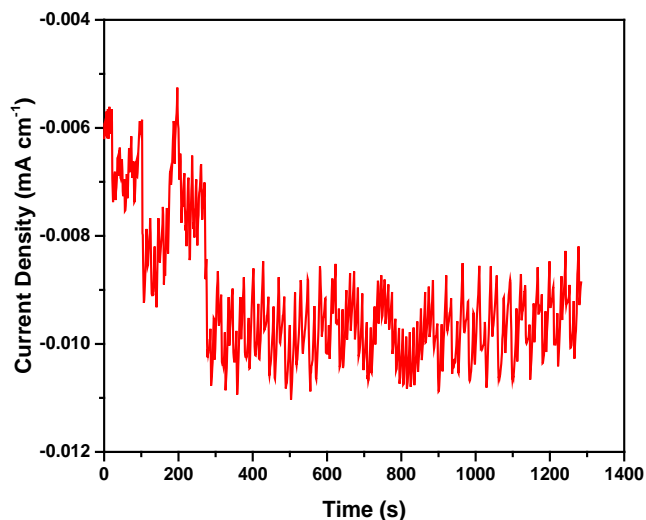


Figure 5.3: Chronoamperometry testing at 0.12 V RHE

It is clear that there is current fluctuation from the flowcell. This could be a result of bubbles filling the small chamber and blocking access to the electrode. Figure 5.4 below shows the concentration and faradaic efficiency at four different cathode potentials. As expected, the concentration decreases as the potential shifts closer to the thermodynamic potential. The selectivity however, follows an unexpected trend, the greatest selectivity isn't seen at the lowest overpotential, it is seen at the highest overpotential. The selectivity makes a 'U' shape. The cause of this is unknown.

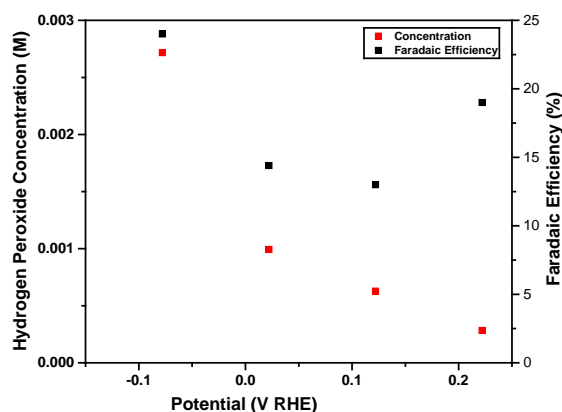


Figure 5.4: Concentration and Efficiency using Ir on Ti Mesh as the anode

5.3 Revised Testing

A change to the configuration of the cell was made considering the results of the first test. The performance of the cell could be better than the performance seen in the initial configuration. As previously discussed, resistance should be minimized if possible. To do this, the anode compartment was removed from the cell. Removing the

anode compartment means that the anode will have to be moved. The new configuration can be seen in Figure 5.5.

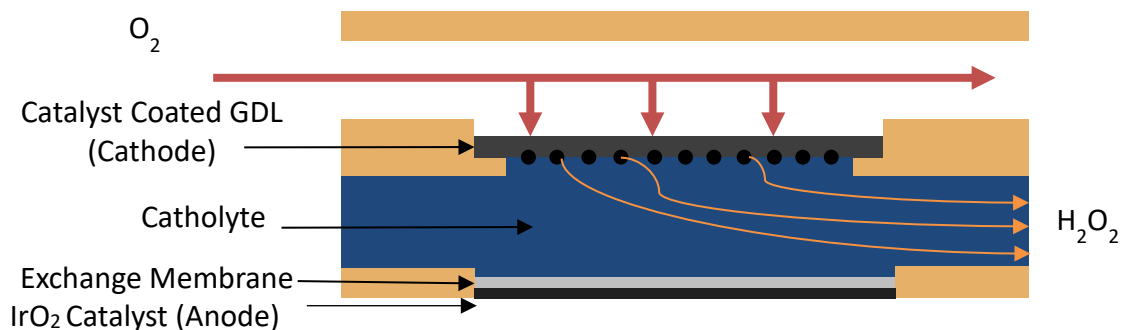


Figure 5.5: Revised flow cell schematic

Nafion membranes soak up water, similar to a sponge. If they did not do this, the anode compartment could not be eliminated. Water that is soaked up by the membrane can react once it reaches the catalyst surface. Iridium can still be used as the catalyst in this situation. Instead of dipcoating the Ir catalyst, it will be spray coated onto the membrane itself. The sprayed portion of the membrane will be oriented towards the outside of the cell. This will help reduce the chances that any product is oxidized.

Figure 5.6 below shows the concentration and efficiency of the new configuration. This graph is expected based on RDE testing and Koutecky-Levich plots. The selectivity increases as the potential nears the thermodynamic potential. In addition to this, the current and concentration increase as the potential goes away from the thermodynamic potential. The concentration slightly decreases from 0 V RHE to -0.1 V RHE, but the decrease is very slight, under (10%), and could be attributed to many different factors.

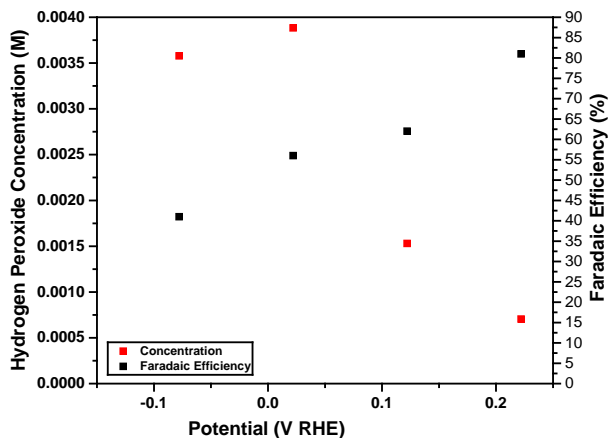


Figure 5.6: Concentration and efficiency using Ir sprayed on membrane as the anode

Using Equation 10, it would only take about 40 minutes to produce enough peroxide to be used by Hammond *et al.* This is a significant improvement over the RDE, as expected. It should be noted that all MFC testing was done with a previous iteration of the catalyst, one that didn't perform as well in RDE testing as either NDC_80 or NDC_100. An increase in both the selectivity and the total production would be expected if the catalyst change was made and the system was retested.

Chapter 6

CONCLUSIONS AND RECOMMENDATIONS

6.1 Conclusions

In this thesis, novel catalysts have been developed and characterized for the oxygen reduction reaction to hydrogen peroxide. These nitrogen doped carbon based catalysts were fundamentally tested in a rotating disk electrode setup. In addition to this, the catalyst was tested in a micro flow cell reactor.

6.1.1 NDC Catalyst

In chapter 3, NDC catalysts were successfully synthesized from KIT-6, a mesoporous silica, using the nanocasting technique. Structural characterization of the template was performed using techniques such as PXRD and N₂ adsorption. The PXRD results verified that structure of the KIT-6 and also confirmed that the pore size changes with changes in calcination temperature. As the calcination temperature increases, the pore size increases as well. Electrochemical surface area was also determined in this work using double layer capacitance. The surface area is correlated with the pore size of the template. Surface area increases as template pore size decreases. In theory, a smaller pore size on the template should lead to a larger exposed area on the resulting catalyst. This however, does not seem to be the case as the pore size didn't influence the BET surface area of the catalyst

6.1.2 Oxygen Reduction

In chapter 4, the ORR reaction was tested using a Rotating Disk Electrode setup. It was found that NDC_80, the NDC catalyst that was synthesized from the smallest pore size template was the overall catalyst. That same template was found to have the largest electrochemical surface area. The second best catalyst was NDC_100, synthesized from the template with the second largest pore size. The selectivity of these two catalysts was measured using Koutecky-Levich plots. It was found that the selectivity of NDC_80 was stable at ~84% throughout the entire range of tested potentials. The selectivity of NDC_100 was not constant, and decreased from 99% at 0.3 V RHE to 78% at 0.0 V RHE. The 99% selectivity is among the highest selectivities reported in literature for this reaction. The selectivity was combined with the total current density to find the partial current density. This allows us to directly compare the two catalysts in terms of production. At potentials less than 0.25 V RHE, NDC_80 is the most productive catalyst, even if it isn't the most efficient. In a RDE setup it would take over 4 hours at the best rate to produce enough H₂O₂ to be used in methane partial oxidation experiments. Rotating Disk Electrodes are used for fundamental research, not for practical production of products. When the rotating speed is increased in the RDE, the total current increases. This happens because the mass transport of reactants is increased to the catalyst surface. Therefore a flow cell was used in an effort to increase mass transport to the catalyst surface

6.1.3 Micro Flow Cell

In chapter 5, a micro flow cell was designed and tested for the ORR reaction. This flow cell can greatly increase the transport of reactants to the catalyst surface. Initially, the flow cell was designed with 3 compartments: gas, cathode, and anode. The anode was Ir dipcoated on Ti-mesh. That configuration did not produce products at a rate that was needed for the methane activation experiments. A change was made in the configuration. The anode compartment was removed in an effort to reduce total cell resistance. By reducing the resistance, higher currents can be achieved at smaller over potentials. The Ir catalyst was sprayed onto the Nafion membrane. Using this configuration, the production rate increased over 25% from the original configuration, and it reduces the time needed to produce enough peroxide for the experiments from 4 hours to 40 minutes.

6.2 Recommendations

There are a number of recommendations that come as a result of this work. There are further investigations needed into the structure of the mesoporous NDC. TEM imaging would be helpful to help confirm the mesoporous structure of the catalyst. In addition to this, XPS can be used to look at the surface chemistry. It has been reported that different types of nitrogen groups such as pyrrolic, pyridinic, and quarternary are responsible for oxygen reduction⁵⁷. Knowing the types of nitrogen would be invaluable in understanding the current catalysts, as that information could be used to design a better catalyst. There are smaller experimental synthesis changes that could be made to change the catalyst. These changes include: the precursor,

calcination temperature, and precursor amount. Although these changes are small, they could have an impact on the final synthesized catalyst⁵⁸⁻⁵⁹.

Another area that needs to be further explored is the design of the micro flow cell.

Many of the production rates were calculated using 25 cm² as the electrode area. The actual surface area tested was only 1 cm². It was assumed that 25 cm² would be an easy scale-up, but it might not be. The shape of the electrode chamber could be an important factor in the design of the flow cell. The cell was designed to be thin to help limit resistance. The inlet/outlet tubing is very small to fit within the chamber.

Increasing the number of outlets or reshaping the chamber might help ensure that any gas in the cathode chamber is efficiently removed. There are other catalyst changes that can be made as well. Cathode loading was chosen to be the same as in RDE experiments. It could be increased in an effort to increase the current. In addition, increasing anode catalyst loading could also help the overall total current.

Methane activation wasn't discussed in this work, but it is a very important part of the work as a whole. Hammond *et al.* only used a small autoclave reactor for the experiments. This reactor only used 10 mL of 0.5M H₂O₂ and produced very little methanol. An ideal reactor would be a flow reactor, possibly a packed bed reactor. The catalyst developed should be suitable for this type of reactor, however it will have to be tested. Na₂SO₄ was used in the ORR experiments, while Hammond used plain water. If the methane catalyst is not compatible with Na₂SO₄ then either a separation must occur before the activation, or another catalyst must be used. In addition to this, a separation will have to be made after the oxidation to acquire usable methanol.

REFERENCES

1. Lunsford, J. H., Catalytic conversion of methane to more useful chemicals and fuels: a challenge for the 21st century. *Catalysis Today* **2000**, *63* (2), 165-174.
2. Spinner, N.; Mustain, W. E., Electrochemical methane activation and conversion to oxygenates at room temperature. *Journal of The Electrochemical Society* **2013**, *160* (11), F1275-F1281.
3. Stoukides, M., Electrochemical studies of methane activation. *Journal of applied electrochemistry* **1995**, *25* (10), 899-912.
4. Ogura, K.; Migita, C.; Ito, Y., Combined photochemical and electrochemical oxidation of methane. *Journal of The Electrochemical Society* **1990**, *137* (2), 500-503.
5. Parmaliana, A.; Frusteri, F.; Arena, F.; Giordano, N., Selective partial oxidation of light paraffins with hydrogen peroxide on thin-layer supported Nafion-H catalysts. *Catalysis letters* **1992**, *12* (4), 353-359.
6. Frese Jr, K. W., Partial electrochemical oxidation of methane under mild conditions. *Langmuir* **1991**, *7* (1), 13-15.
7. Promoppatum, P.; Viswanathan, V., Identifying Material and Device Targets for a Flare Gas Recovery System Utilizing Electrochemical Conversion of Methane to Methanol. *ACS Sustainable Chemistry & Engineering* **2016**, *4* (3), 1736-1745.
8. EPA, U. S., U.S. Methane Emissions, By Source. 2014.
9. Initiative, G. M., Global Methane Emissions by Sector. 2016.
10. Boucher, O.; Friedlingstein, P.; Collins, B.; Shine, K. P., The indirect global warming potential and global temperature change potential due to methane oxidation. *Environmental Research Letters* **2009**, *4* (4), 044007.
11. Tollefson, J., Oil boom raises burning issues. *Nature* **2013**, *495* (7441), 290-1.
12. Wogan, D., North Dakota flared off \$1 billion worth of natural gas last year. *Scientific America Blogs* **2013**.

13. Xu, J.; Froment, G. F., Methane steam reforming, methanation and water-gas shift: I. Intrinsic kinetics. *AIChE journal* **1989**, *35* (1), 88-96.
14. Yang, C.; Ma, Z.; Zhao, N.; Wei, W.; Hu, T.; Sun, Y., Methanol synthesis from CO₂-rich syngas over a ZrO₂ doped CuZnO catalyst. *Catalysis Today* **2006**, *115* (1), 222-227.
15. Alvarado, M. The Changing Face of the Global Methanol Industry *IHS Chemical Bulletin* [Online], 2016. (accessed 07/07/2017).
16. Hammond, C.; Forde, M. M.; Rahim, A.; Hasbi, M.; Thetford, A.; He, Q.; Jenkins, R. L.; Dimitratos, N.; Lopez-Sanchez, J. A.; Dummer, N. F., Direct Catalytic Conversion of Methane to Methanol in an Aqueous Medium by using Copper-Promoted Fe-ZSM-5. *Angewandte Chemie International Edition* **2012**, *51* (21), 5129-5133.
17. Hammond, C.; Jenkins, R. L.; Dimitratos, N.; Lopez-Sanchez, J. A.; ab Rahim, M. H.; Forde, M. M.; Thetford, A.; Murphy, D. M.; Hagen, H.; Stangland, E. E., Catalytic and Mechanistic Insights of the Low-Temperature Selective Oxidation of Methane over Cu-Promoted Fe-ZSM-5. *Chemistry-a European Journal* **2012**, *18* (49), 15735-15745.
18. Campos-Martin, J. M.; Blanco-Brieva, G.; Fierro, J. L., Hydrogen peroxide synthesis: an outlook beyond the anthraquinone process. *Angewandte Chemie International Edition* **2006**, *45* (42), 6962-6984.
19. Santacesaria, E.; Di Serio, M.; Russo, A.; Leone, U.; Velotti, R., Kinetic and catalytic aspects in the hydrogen peroxide production via anthraquinone. *Chemical engineering science* **1999**, *54* (13-14), 2799-2806.
20. Glaze, W. H.; Kang, J.-W.; Chapin, D. H., The chemistry of water treatment processes involving ozone, hydrogen peroxide and ultraviolet radiation. **1987**.
21. Goi, A.; Trapido, M., Hydrogen peroxide photolysis, Fenton reagent and photo-Fenton for the degradation of nitrophenols: a comparative study. *Chemosphere* **2002**, *46* (6), 913-922.
22. Chai, X.-S.; Hou, Q.; Luo, Q.; Zhu, J., Rapid determination of hydrogen peroxide in the wood pulp bleaching streams by a dual-wavelength spectroscopic method. *Analytica chimica acta* **2004**, *507* (2), 281-284.
23. Watt, B. E.; Proudfoot, A. T.; Vale, J. A., Hydrogen peroxide poisoning. *Toxicological reviews* **2003**, *23* (1), 51-57.

24. Walling, C., Fenton's reagent revisited. *Accounts of chemical research* **1975**, *8* (4), 125-131.
25. Qiang, Z.; Chang, J.-H.; Huang, C.-P., Electrochemical generation of hydrogen peroxide from dissolved oxygen in acidic solutions. *Water Research* **2002**, *36* (1), 85-94.
26. Berglin, T.; Schoeoen, N. H., Selectivity aspects of the hydrogenation stage of the anthraquinone process for hydrogen peroxide production. *Industrial & Engineering Chemistry Process Design and Development* **1983**, *22* (1), 150-153.
27. SUDO, M.; KITAGUCHI, H.; KOIDE, K., Electrochemical production of hydrogen peroxide by reduction of oxygen. *Journal of chemical engineering of Japan* **1985**, *18* (5), 409-414.
28. Liang, Y.; Li, Y.; Wang, H.; Zhou, J.; Wang, J.; Regier, T.; Dai, H., Co₃O₄ nanocrystals on graphene as a synergistic catalyst for oxygen reduction reaction. *Nature materials* **2011**, *10* (10), 780-786.
29. Guillet, N.; Roué, L.; Marcotte, S.; Villers, D.; Dodelet, J.; Chhim, N.; Vin, S. T., Electrogeneration of hydrogen peroxide in acid medium using pyrolyzed cobalt-based catalysts: influence of the cobalt content on the electrode performance. *Journal of applied electrochemistry* **2006**, *36* (8), 863-870.
30. Marcotte, S.; Villers, D.; Guillet, N.; Roué, L.; Dodelet, J., Electroreduction of oxygen on Co-based catalysts: determination of the parameters affecting the two-electron transfer reaction in an acid medium. *Electrochimica Acta* **2004**, *50* (1), 179-188.
31. Verdaguer-Casadevall, A.; Deiana, D.; Karamad, M.; Siahrostami, S.; Malacrida, P.; Hansen, T. W.; Rossmeisl, J.; Chorkendorff, I.; Stephens, I. E., Trends in the electrochemical synthesis of H₂O₂: Enhancing activity and selectivity by electrocatalytic site engineering. *Nano letters* **2014**, *14* (3), 1603-1608.
32. Jirkovský, J. S.; Panas, I.; Ahlberg, E.; Halasa, M.; Romani, S.; Schiffrin, D. J., Single atom hot-spots at Au–Pd nanoalloys for electrocatalytic H₂O₂ Production. *Journal of the American Chemical Society* **2011**, *133* (48), 19432-19441.
33. Barros, W. R.; Reis, R. M.; Rocha, R. S.; Lanza, M. R., Electrogeneration of hydrogen peroxide in acidic medium using gas diffusion electrodes modified with cobalt (II) phthalocyanine. *Electrochimica Acta* **2013**, *104*, 12-18.

34. Siahrostami, S.; Verdaguer-Casadevall, A.; Karamad, M.; Deiana, D.; Malacrida, P.; Wickman, B.; Escudero-Escribano, M.; Paoli, E. A.; Frydendal, R.; Hansen, T. W., Enabling direct H₂O₂ production through rational electrocatalyst design. *Nature materials* **2013**, *12* (12), 1137-1143.
35. Dilimon, V.; Narayanan, N. V.; Sampath, S., Electrochemical reduction of oxygen on gold and boron-doped diamond electrodes in ambient temperature, molten acetamide–urea–ammonium nitrate eutectic melt. *Electrochimica Acta* **2010**, *55* (20), 5930-5937.
36. dos Reis, F. V.; Antonin, V. S.; Hammer, P.; Santos, M. C.; Camargo, P. H., Carbon-supported TiO₂–Au hybrids as catalysts for the electrogeneration of hydrogen peroxide: Investigating the effect of TiO₂ shape. *Journal of Catalysis* **2015**, *326*, 100-106.
37. Edwards, J. K.; Pritchard, J.; Lu, L.; Piccinini, M.; Shaw, G.; Carley, A. F.; Morgan, D. J.; Kiely, C. J.; Hutchings, G. J., The Direct Synthesis of Hydrogen Peroxide Using Platinum-Promoted Gold–Palladium Catalysts. *Angewandte Chemie International Edition* **2014**, *53* (9), 2381-2384.
38. Sidik, R. A.; Anderson, A. B.; Subramanian, N. P.; Kumaraguru, S. P.; Popov, B. N., O₂ reduction on graphite and nitrogen-doped graphite: experiment and theory. *The Journal of Physical Chemistry B* **2006**, *110* (4), 1787-1793.
39. Fellingner, T.-P.; Hasché, F. d. r.; Strasser, P.; Antonietti, M., Mesoporous nitrogen-doped carbon for the electrocatalytic synthesis of hydrogen peroxide. *Journal of the American Chemical Society* **2012**, *134* (9), 4072-4075.
40. Hasché, F.; Oezaslan, M.; Strasser, P.; Fellingner, T.-P., Electrocatalytic hydrogen peroxide formation on mesoporous non-metal nitrogen-doped carbon catalyst. *Journal of Energy Chemistry* **2016**, *25* (2), 251-257.
41. Perazzolo, V.; Durante, C.; Pilot, R.; Paduano, A.; Zheng, J.; Rizzi, G. A.; Martucci, A.; Granozzi, G.; Gennaro, A., Nitrogen and sulfur doped mesoporous carbon as metal-free electrocatalysts for the in situ production of hydrogen peroxide. *Carbon* **2015**, *95*, 949-963.
42. Wei, W.; Liang, H.; Parvez, K.; Zhuang, X.; Feng, X.; Müllen, K., Nitrogen-Doped Carbon Nanosheets with Size-Defined Mesopores as Highly Efficient Metal-Free Catalyst for the Oxygen Reduction Reaction. *Angewandte Chemie* **2014**, *126* (6), 1596-1600.

43. Liu, Y.; Quan, X.; Fan, X.; Wang, H.; Chen, S., High-Yield Electrosynthesis of Hydrogen Peroxide from Oxygen Reduction by Hierarchically Porous Carbon. *Angewandte Chemie International Edition* **2015**, *54* (23), 6837-6841.
44. Park, J.; Nabae, Y.; Hayakawa, T.; Kakimoto, M.-a., Highly selective two-electron oxygen reduction catalyzed by mesoporous nitrogen-doped carbon. *ACS Catalysis* **2014**, *4* (10), 3749-3754.
45. Lee, Y.-H.; Li, F.; Chang, K.-H.; Hu, C.-C.; Ohsaka, T., Novel synthesis of N-doped porous carbons from collagen for electrocatalytic production of H₂O₂. *Applied Catalysis B: Environmental* **2012**, *126*, 208-214.
46. Jones, B. H.; Lodge, T. P., Nanocasting nanoporous inorganic and organic materials from polymeric bicontinuous microemulsion templates. *Polymer journal* **2012**, *44* (2), 131-146.
47. Rosen, J.; Hutchings, G. S.; Jiao, F., Ordered mesoporous cobalt oxide as highly efficient oxygen evolution catalyst. *Journal of the American Chemical Society* **2013**, *135* (11), 4516-4521.
48. Kleitz, F.; Choi, S. H.; Ryoo, R., Cubic Ia 3 d large mesoporous silica: synthesis and replication to platinum nanowires, carbon nanorods and carbon nanotubes. *Chemical Communications* **2003**, (17), 2136-2137.
49. Song, Y.; Peng, R.; Hensley, D. K.; Bonnesen, P. V.; Liang, L.; Wu, Z.; Meyer, H. M.; Chi, M.; Ma, C.; Sumpter, B. G., High-Selectivity Electrochemical Conversion of CO₂ to Ethanol using a Copper Nanoparticle/N-Doped Graphene Electrode. *ChemistrySelect* **2016**, *1* (19), 6055-6061.
50. Thorson, M. R.; Siil, K. I.; Kenis, P. J., Effect of Cations on the Electrochemical Conversion of CO₂ to CO. *Journal of the Electrochemical Society* **2013**, *160* (1), F69-F74.
51. Sellers, R. M., Spectrophotometric determination of hydrogen peroxide using potassium titanium (IV) oxalate. *Analyst* **1980**, *105* (1255), 950-954.
52. Lu, A. H.; Schüth, F., Nanocasting: a versatile strategy for creating nanostructured porous materials. *Advanced Materials* **2006**, *18* (14), 1793-1805.
53. Yonemoto, B. T. Nanoporous materials for energy applications. University of Delaware, 2015.

54. Pirez, C.; Caderon, J.-M.; Dacquin, J.-P.; Lee, A. F.; Wilson, K., Tunable KIT-6 mesoporous sulfonic acid catalysts for fatty acid esterification. *ACS catalysis* **2012**, *2* (8), 1607-1614.
55. Yamanaka, I.; Onizawa, T.; Takenaka, S.; Otsuka, K., Direct and Continuous Production of Hydrogen Peroxide with 93% Selectivity Using a Fuel-Cell System. *Angewandte Chemie International Edition* **2003**, *42* (31), 3653-3655.
56. Luc, W.; Rosen, J.; Jiao, F., An Ir-based anode for a practical CO₂ electrolyzer. *Catalysis Today* **2017**, *288*, 79-84.
57. Chen, L.; Xu, C.; Du, R.; Mao, Y.; Xue, C.; Chen, L.; Qu, L.; Zhang, J.; Yi, T., Rational design of three-dimensional nitrogen-doped carbon nanoleaf networks for high-performance oxygen reduction. *Journal of Materials Chemistry A* **2015**, *3* (10), 5617-5627.
58. Liu, N.; Yin, L.; Wang, C.; Zhang, L.; Lun, N.; Xiang, D.; Qi, Y.; Gao, R., Adjusting the texture and nitrogen content of ordered mesoporous nitrogen-doped carbon materials prepared using SBA-15 silica as a template. *Carbon* **2010**, *48* (12), 3579-3591.
59. Vinu, A.; Ariga, K.; Mori, T.; Nakanishi, T.; Hishita, S.; Golberg, D.; Bando, Y., Preparation and Characterization of Well-Ordered Hexagonal Mesoporous Carbon Nitride. *Advanced materials* **2005**, *17* (13), 1648-1652.

Appendix

COPYRIGHT PERMISSIONS

This appendix contains the copyright permissions for all figures reproduced in this thesis

Permission to adapt Figure 1.3

JOHN WILEY AND SONS LICENSE TERMS AND CONDITIONS

Jul 06, 2017

This Agreement between University of Delaware – Andrew Craft ("You") and John Wiley and Sons ("John Wiley and Sons") consists of your license details and the terms and conditions provided by John Wiley and Sons and Copyright Clearance Center.

License Number	4143230926073
License date	Jul 06, 2017
Licensed Content Publisher	John Wiley and Sons
Licensed Content Publication	Angewandte Chemie International Edition
Licensed Content Title	Direct Catalytic Conversion of Methane to Methanol in an Aqueous Medium by using Copper-Promoted Fe-ZSM-5
Licensed Content Author	Ceri Hammond, Michael M. Forde, Mohd Hasbi Ab Rahim, Adam Thetford, Qian He, Robert L. Jenkins, Nikolaos Dimitratos, Jose A. Lopez-Sanchez, Nicholas F. Dummer, Damien M. Murphy, Albert F. Carley, Stuart H. Taylor, David J. Willock, Eric E. Stangland, Joo Kang, Henk Hagen, Christopher J. Kiely, Graham J. Hutchings
Licensed Content Date	Apr 5, 2012
Licensed Content Pages	5
Type of Use	Dissertation/Thesis
Requestor type	University/Academic
Format	Print and electronic
Portion	Figure/table
Number of figures/tables	1
Original Wiley figure/table number(s)	Figure 1 C
Will you be translating?	No
Title of your thesis / dissertation	Nitrogen Doped Carbon Catalyst for the Oxygen Reduction Reaction to be used for Methane Partial Oxidation
Expected completion date	Jul 2017
Expected size (number of pages)	60
Requestor Location	University of Delaware 150 Academy Street Newark, 19716 United Kingdom Attn: University of Delaware
Publisher Tax ID	EU826007151
Billing Type	Invoice
Billing Address	University of Delaware 150 Academy Street Newark, United Kingdom 19716 Attn: University of Delaware
Total	0.00 USD
Terms and Conditions	

Permission to adapt Figure 3.2



RightsLink®

Home

Create Account

Help



ACS Publications
Most Trusted. Most Cited. Most Read.

Title: Tunable KIT-6 Mesoporous Sulfonic Acid Catalysts for Fatty Acid Esterification
Author: Cyril Pirez, Jean-Michel Caderon, Jean-Philippe Dacquin, et al
Publication: ACS Catalysis
Publisher: American Chemical Society
Date: Aug 1, 2012

Copyright © 2012, American Chemical Society

LOGIN

If you're a [copyright.com](#) user, you can login to RightsLink using your [copyright.com](#) credentials. Already a [RightsLink user](#) or want to [learn more?](#)

PERMISSION/LICENSE IS GRANTED FOR YOUR ORDER AT NO CHARGE

This type of permission/license, instead of the standard Terms & Conditions, is sent to you because no fee is being charged for your order. Please note the following:

- Permission is granted for your request in both print and electronic formats, and translations.
- If figures and/or tables were requested, they may be adapted or used in part.
- Please print this page for your records and send a copy of it to your publisher/graduate school.
- Appropriate credit for the requested material should be given as follows: "Reprinted (adapted) with permission from (COMPLETE REFERENCE CITATION). Copyright (YEAR) American Chemical Society." Insert appropriate information in place of the capitalized words.
- One-time permission is granted only for the use specified in your request. No additional uses are granted (such as derivative works or other editions). For any other uses, please submit a new request.

If credit is given to another source for the material you requested, permission must be obtained from that source.

BACK

CLOSE WINDOW

Copyright © 2017 [Copyright Clearance Center, Inc.](#) All Rights Reserved. [Privacy statement](#), [Terms and Conditions](#).

Comments? We would like to hear from you. E-mail us at customercare@copyright.com